Scalable, Ultrathin, and High-Temperature-Resistant Solid Polymer Electrolytes for Energy-Dense Lithium Metal Batteries

*Yinxing Ma, Jiayu Wan, Yufei Yang, Yusheng Ye, Xin Xiao, David T. Boyle, Will Burke, Zhuojun Huang, Hao Chen, Yi Cui, Zhiao Yu, Solomon T. Oyakhire, and Yi Cui**

All-solid-state batteries (ASSBs) demonstrate great promise, offering high energy density, good thermal stability, and safe operation compared with traditional Li-ion batteries. Among various solid-state electrolytes (SSEs), solid polymer electrolytes (SPEs) offer an attractive choice due to their thinness, low density, and good manufacturability. However, ultrathin SPEs that work with practical current densities or at high temperatures remain challenging, limiting applicable conditions of SPE-based batteries. Here, the authors report a novel scalable, ultrathin, and high-temperature-resistant SPE for ASSBs. This design includes an electrospun polyacrylonitrile (PAN) matrix and polyethylene oxide (PEO)/Li salt ionic conductor, which offers a stable LiF and Li_3N containing SSE/Li interface. The unique interface—as well as the good mechanical strength—inhibits lithium dendrites and prevents short circuiting. As a result, symmetrical Li—Li cells deliver more than 300 h cyclability at 0.5 mA cm^{-2}. ASSBs fabricated with only 5 µm-thickness PAN-PEO/lithium bis(trifluoromethanesulfonyl)imide reach 300 cycles at 0.3 C rate at 60 °C. The excellent thermal stability of PAN also results in safer SPEs at high temperatures. The design extends battery operation up to temperatures of 120 and 150 °C, where it achieves 500 cycles at C/2 rate and 100 cycles at 2C rate, respectively.

1. Introduction

The commercialization of rechargeable lithium-ion batteries (LIBs) has revolutionized the modern lifestyle,[1] leading society into an electrified, wireless, and sustainable future. With the continuous upsurge in demand for energy-dense devices, future advancement of batteries will require higher energy density, longer cycle life, and better safety.[2,3] Lithium metal anodes have a high specific capacity of ≈3800 mAh g^{-1},[4,5] enabling the possibility of higher energy density batteries. However, commonly used liquid electrolytes in Li metal batteries (LMBs) often result in uncontrollable lithium dendrite growth, inadequate electrochemical and thermal stability, and high flammability.[2,4] As a result, limited performance and safety issues restrict the application and development of LMBs based on conventional liquid electrolytes.

Compared to liquid electrolytes, solid-state electrolytes (SSEs) can potentially provide better safety, higher mechanical strength, and excellent chemical and electrochemical stability.[4,6–10] SSEs can be grouped into three categories: inorganic solid electrolytes,[11–14] solid polymer electrolytes (SPEs),[15–17] and their hybrids.[18–21] Among them, inorganic solid electrolytes have the highest ionic conductivity[11] and excellent thermal stability,[2] but their interfacial compatibility, brittleness, and rigidity[22,23] are the challenges to be addressed towards their practical application.[9] In contrast, SPEs have good interfacial compatibility,[24] and excellent chemical and electrochemical stability,[18,24,25] but are lacking in thermal stability and mechanical strength, which generally makes them insufficient for meeting the requirements of high-safety and high-performance LMBs,[6,26,27] especially at high temperatures (>100 °C).[28] A hybrid of ceramic and polymer SSEs may offer good mechanical strength and safety, but it is still challenging to achieve ultrathin composite SSEs. Therefore, the design of a robust, ultrathin SSE that fulfills the above requirements is urgently needed.

To achieve an energy density comparable to or larger than liquid electrolyte-based cells, ultrathin and lightweight solid electrolytes are necessary.[29,30] Compared to typical, thick ceramic electrolytes with thicknesses in the range of a few hundred microns,[14,31–33] SPEs and their composites are easily engineered and manufacturable for tunable smaller

Y. Ma
College of Chemistry and Chemical Engineering
iChEM
Xiamen University
Xiamen 361005, P. R. China

Y. Ma, J. Wan, Y. Yang, Y. Ye, X. Xiao, W. Burke, Z. Huang, H. Chen, Y. Cui, Y. Cui
Department of Materials Science and Engineering
Stanford University
Stanford, CA 94305, USA
E-mail: yicui@stanford.edu

D. T. Boyle, Z. Yu
Department of Chemistry
Stanford University
Stanford, CA 94305, USA

Z. Yu, S. T. Oyakhire
Department of Chemical Engineering
Stanford University
Stanford, CA 94305, USA

Y. Cui
Stanford Institute for Materials and Energy Sciences
SLAC National Accelerator Laboratory
2575 Sand Hill Road, Menlo Park, CA 94025, USA

The ORCID identification number(s) for the author(s) of this article can be found under https://doi.org/10.1002/aenm.202103720.

DOI: 10.1002/aenm.202103720

thickness.[16,34–36] Robust, thin, porous polymers have been previously used as structured support for filling in SPEs, such as polyethylene oxide (PEO)/lithium bis(trifluoromethanesulfonyl) imide (LiTFSI), resulting in ultrathin SPEs.[34,37,38] However, designing a functional ultrathin solid electrolyte for practical current densities and capacities is still challenging. Thin SPEs can have an increased risk of short-circuiting and are still limited by the Li/SPE interfacial stability and high-temperature stability.

In this work, we have prepared an ultrathin polyacrylonitrile (PAN)-PEO/LiTFSI SPE film with a nanofibrous PAN membrane matrix that can overcome the challenges mentioned above. The PAN membrane matrix is easily prepared by electrospinning, followed by calendaring. The calendared PAN membrane has four major functions: 1) the technique combining electrospinning and calendaring is a facile, scalable, and easily manufacturable method to prepare polymer membranes,[39] as the matrix material is easily modified or functionalized. Compared with previously demonstrated polyimide[34] or polyethylene (PE) separator hosts,[37] electrospinning could offer tunable chemical functionality by choosing a variety of polymer chemistries; 2) compared with a previously reported PEO-LiTFSI/electrospun PAN/$Li_{6.7}La_3Zr_{1.7}Ta_{0.3}O_{12}$ composite electrolyte,[40] calendaring gives a PAN membrane a higher volume percentage and modulus, thereby ensuring ultrathin and dense SPEs down to 5 µm, which is one of the thinnest SSEs reported so far;[37] 3) different from porous electrospun polymer films without calendaring, the calendared dense PAN membranes greatly increase the interfacial contact area between PAN fibers and the Li electrode. Thus, a Li_3N and LiF rich SPE/Li interface can be formed, facilitating the stable cycling of Li batteries; and 4) the application of a particularly unique property of PAN that distinguishes it from other polymers—high thermal stability—was not proposed previously. In our work, PAN exhibits high thermal stability to ensure the safe and stable working of all-solid-state batteries at high temperatures up to 150 °C, which substantially exceeds common temperature ranges of SPEs. We studied the unique properties of PAN and applied them to the high-temperature batteries field for the first time, which also fully reflects the novelty of our work. Infiltration of PEO/LiTFSI into a 20 µm PAN membrane matrix gives an ultra-thin PAN-PEO/LiTFSI SPE. This SPE shows good cycling stability in symmetrical Li—Li cells at high current densities of 0.3 and 0.5 mA cm^{-2}. The design benefits from the high mechanical strength of the PAN membrane and its stable SSE|Li interface. We demonstrated the good rate performance and cycling stability at 60 °C even with an ultra-thin thickness of 5 µm. PAN's excellent thermal stability enables all-solid-state batteries that exhibit outstanding cycling efficiency and stability at high temperatures of 120 °C and even 150 °C, much higher than other SPE systems.[28,35,41–43] This provides us with high-safety batteries which can work under high temperature conditions.

2. Results and Discussion

The preparation process of ultrathin SPE is shown in **Figure 1**. Electrospinning and subsequent calendaring (Figure 1a) are able to prepare PAN membranes in a scalable and roll-to-roll fashion (Figure 1b). As-made membranes are uniform, free-standing, and flexible. The calendaring process thins and densifies the PAN membrane, leading to smaller pores and providing larger interfacial contact areas with the electrode (Figure 1a). As shown in Figure 1c,d, the PAN membrane has a 3D network of nanofibrous PAN structures, which are intertwined to form pores with micron or nanometer diameters. Cross-sectional scanning electron microscope (SEM) image (Figure 1e) shows that the surfaces of PAN membranes are flat and uniform, with thicknesses of ≈20 µm, which is a competitive level of thickness for SPEs. The infiltration of PEO/LiTFSI fills the PAN membrane, forming the final SPE (PAN-PEO/LiTFSI) (Figure 1f,g). The PAN fibers and PEO/LiTFSI are both visible on the surface of the electrolyte. The average thickness of the SPE after infiltration is ≈28 µm (Figure 1h). The compact PAN host with micro- and nano-sized pores in the 3D structured membrane is beneficial to inhibit the growth of lithium dendrites. The electrospinning method is therefore convenient, scalable, cost-efficient, generalizable to other polymer chemistries, and versatile from multiple perspectives in preparing ultra-thin solid electrolytes.

The PAN membrane demonstrates an excellent mechanical strength despite its thickness of 20 µm, as demonstrated in the stress–strain curves (**Figure 2**a). The stress of PAN reached ≈50 MPa and the elongation at break was ≈26%. The modulus was ≈1530 MPa, 15 000 times higher than the modulus of PEO/LiTFSI (≈0.1 MPa).[34] Calendaring of the electrospun PAN matrix prior to incorporation of the SPE into battery played a key role in providing such a high modulus. It not only increased the PAN volume percentage of electrospun PAN membrane from 26.1% before calendaring to 81.3% after calendaring, but also increased the compactness and the interaction between PAN fibers, thereby greatly increasing PAN modulus (Figure S1, Supporting Information). This high modulus is very important for increasing the critical current density, allowing for long-duration cell operation and manufacturability. The critical current density is the highest current density at which the Li—Li symmetrical cells can stand before failure (from short circuiting or drastic overpotential increase).[9] At 60 °C, the critical current density of PAN-PEO/LiTFSI based symmetrical Li—Li cell can reach 0.9 mA cm^{-2} at a cycling capacity of 0.45 mAh cm^{-2}, while plain PEO/LiTFSI short circuited at 0.2 mA cm^{-2} (Figure 2b). Such a significant increase in critical current density indicated that the thin, mechanically strong PAN membrane host played a key role. To demonstrate the success of our design, which simultaneously decreases the thickness of the SSEs and increases their critical current density, we compared the critical current densities and corresponding thicknesses of several polymer and polymer-ceramic composite SSEs reported in the literature (Figure 2c). PAN-PEO/LiTFSI exhibited obvious competitiveness in both critical current density and thickness. The critical current density of PAN-PEO/LiTFSI was higher than most SPE-based SSEs. Although it was slightly lower than that of a few SSEs, the thickness of our PAN-PEO/LiTFSI was much thinner than theirs. In addition, the thickness of PAN-PEO/LiTFSI was thinner than most SPE-based SSEs. Although there were a few SSEs thinner than PAN-PEO/LiTFSI, the critical current density of PAN-PEO/LiTFSI was much higher than theirs. It can be seen that the relative ratio of critical current density and thickness of our PAN-PEO/LiTFSI was much higher than that of other SPE-based

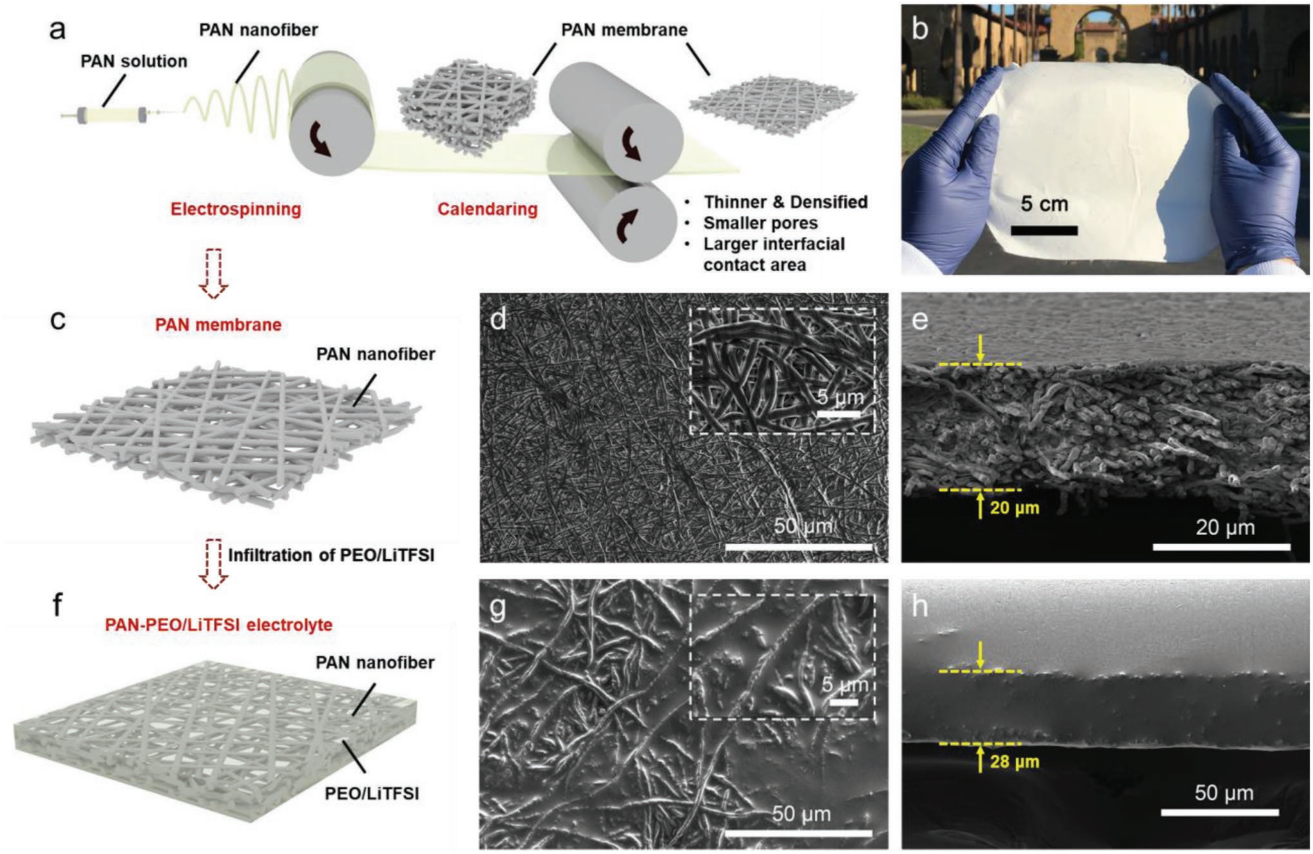

Figure 1. a) Schematic illustration of the preparation of the PAN membrane. b) Photo image of a nanofibrous PAN film. c) Schematic illustration of the PAN membrane. d,e) SEM image of PAN membrane from d) top view (inset shows a typical magnified SEM image of panel (d)) and e) side view before infiltration of PEO/LiTFSI into the electrospun PAN membrane. f) Schematic illustration of PAN-PEO/LiTFSI electrolyte. After infiltration of PEO/LiTFSI into c) PAN membrane, PAN-PEO/LiTFSI SSE was obtained. g,h) SEM image of PAN-PEO/LiTFSI electrolyte from g) top view (inset shows a typical magnified SEM image of panel (g)) and h) side view after infiltration of PEO/LiTFSI into electrospun PAN membrane.

SSEs. Therefore, PAN-PEO/LiTFSI shows an outstanding comprehensive advantage, capable of exhibiting high critical current density with an ultrathin thickness. This indicates that our work provides a novel insight for enabling all-solid-state batteries with both high power and high energy density.

Symmetrical Li—Li cells were also assembled to test long-term cycling at 60 °C. At 0.5 mA cm^{-2} and a cycling capacity of 0.25 mAh cm^{-2}, PAN-PEO/LiTFSI electrolyte can run for 300 cycles (Figure 2d). In contrast, plain PEO/LiTFSI cells short circuited once the current density reached 0.5 mA cm^{-2}. Impressively, the overpotential of symmetrical Li/PAN-PEO/LiTFSI/Li cells stayed below 400 mV during the whole cycling process, only increasing slightly from 380.7 mV for the 1st cycle to 399.3 mV for the 300th cycle with an average increasing rate of only 0.016% per cycle. This indicates that PAN-based solid electrolyte has excellent interfacial stability against Li metal. Another symmetrical Li—Li cell running at 0.3 mA cm^{-2} and 0.15 mAh cm^{-2} also functioned well for more than 600 cycles (Figure S2, Supporting Information). For this test, the overpotential was averaged at ≈150 mV, with negligible change during the entire range of testing; 124.6 mV was recorded for the 1st cycle and 170.5 mV for the 600th, for an average increasing rate of only 0.06% per cycle. The analogous symmetrical Li/PEO/LiTFSI/Li cell, on the other hand, still short-circuited after increasing the current density. This Li—Li symmetrical cell data supports that our PAN-based solid electrolyte can work stably at high current densities.

The stability between SSE and Li metal can be evaluated by the change of the interfacial resistance. As shown in **Figure 3**a, the initial interfacial resistance between PAN-based SSE and Li metal was much lower than that of Li|PEO/LiTFSI interface at 60 °C, only increased slightly with time, and stabilized after 40 h. In contrast, the interfacial resistance between PEO/LiTFSI and Li metal increased dramatically and was still not stabilized after 40 h. This result provides strong evidence for the good stability between our PAN-based electrolyte and Li metal, which can be attributed to the improved interfacial chemistry between the SSE and Li metal, as illustrated in Figure 3b. The formation of inorganic, stable, and highly ionic conductive Li_3N at the Li|PAN-PEO/LiTFSI interface plays a key role in stabilizing it. LiF can also be observed for both the Li|PEO/LiTFSI interface and Li|PAN-PEO/LiTFSI interface since it is demonstrated to be formed in PEO/LiTFSI-based electrolytes during cycling.[44–46]

We studied the interface between PAN-based electrolyte and Li metal by X-ray photoelectron spectroscopy (XPS). In XPS spectra of PAN (Figure S3, Supporting Information), the C 1s

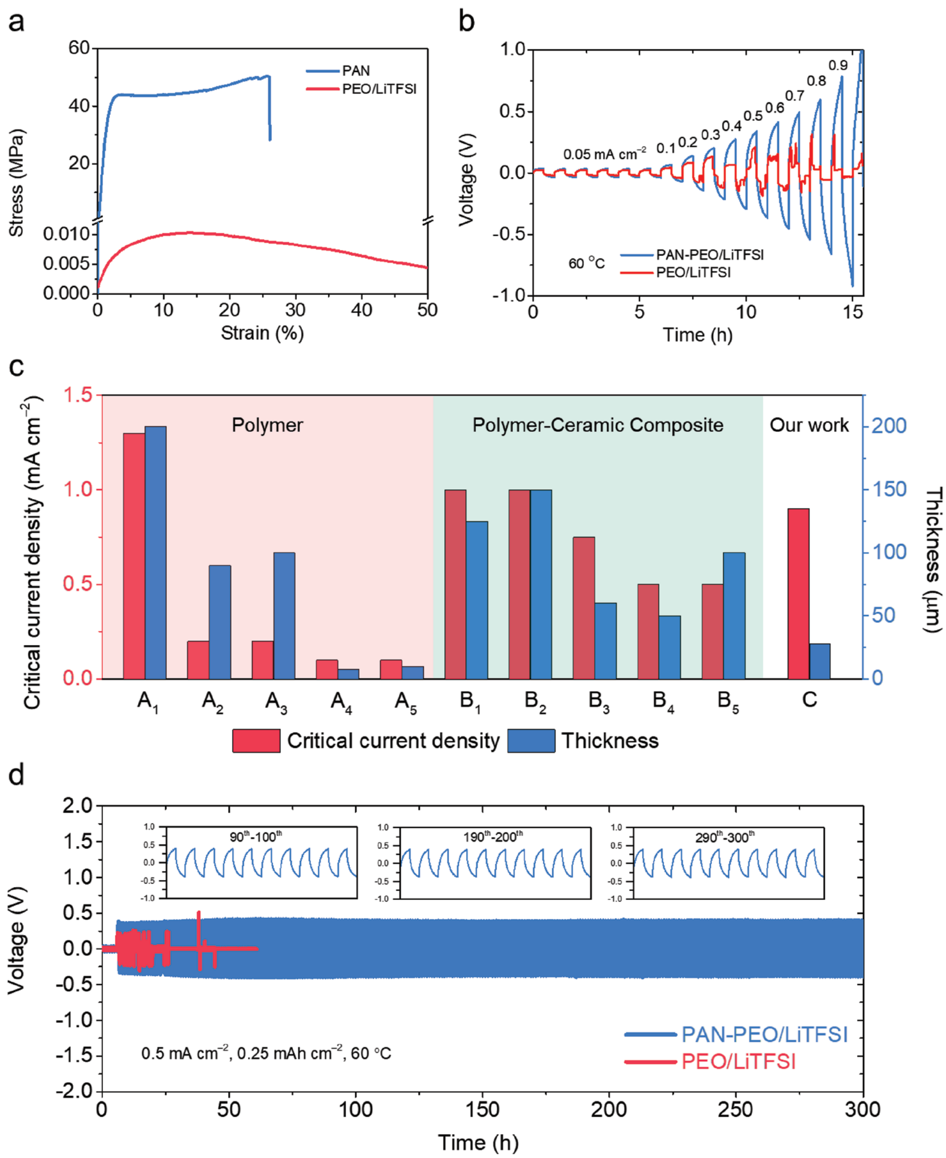

Figure 2. a) Stress–strain curves of PAN membrane and PEO/LiTFSI film.[34] b) Critical current density of PAN-PEO/LiTFSI and PEO/LiTFSI at 60 °C. c) Critical current density and corresponding thickness chart of different SSEs. A_1–A_5 denote polymer SSEs, B_1–B_5 denote polymer/ceramic composites SSEs. See Table S1, Supporting Information, for details. d) Long-term cycling at 0.5 mA cm^{-2} of symmetrical Li–Li cells with PAN-PEO/LiTFSI electrolyte and PEO/LiTFSI SPE at 60 °C. Inset: voltage profile of Li/PAN-PEO/LiTFSI/Li from 90th to 100th cycles, from 190th to 200th cycles, and from 290th to 300th cycles. Each cycle lasts for 1 h.

peak at 284.8 eV and the N 1s peak at 397.9 eV correspond to C≡N moieties, while the C 1s peak at 283.5 eV originate from aliphatic C—C bonds. In XPS spectra of PAN-PEO/LiTFSI|Li interface (Figure 3c–h), these peaks of PAN disappeared. As shown in Figure 3c–h, the C1s peak at 286.6 and 284.8 eV, and O 1s peak at 532.9 eV were from PEO, while the C 1s peak at 292.7 eV, N 1s peak at 399.0 eV, F 1s peak at 688.5 eV, and S 2p peak at 168.5 eV corresponded to LiTFSI. After cycling, both LiF and Li_3N were found at PAN-PEO/LiTFSI|Li interface. The N 1s peak at 397.2 eV and Li 1s peak at 55.0 eV corresponded to Li_3N, while Li 1s peak at 56.2 eV and F 1s peak at 684.7 eV corresponded to LiF. To clarify the chemical origin of Li_3N and LiF, we also studied the interface between PEO/LiTFSI and Li metal by XPS. As shown in Figure S4, Supporting Information, different from XPS of PAN-PEO/LiTFSI|Li interface, only LiF was observed in the PEO/LiTFSI|Li interface, without Li_3N, which is consistent with XPS results demonstrated in previous works on PEO/LiTFSI.[44–46] Therefore, LiTFSI leads to form LiF and PAN leads to the formation of Li_3N at the PAN-PEO/LiTFSI|Li interface. The presence of the unique Li_3N is of significant importance in reducing interfacial resistance and preventing lithium dendrite growth by maintaining a uniform distribution of Li ions at the interface, since it is not only a superionic Li^+ conductor but also allows for good wettability with Li metal electrode.[47–52] Besides, Li_3N also has superior stability against Li metal, which can help mitigate continuous side reactions

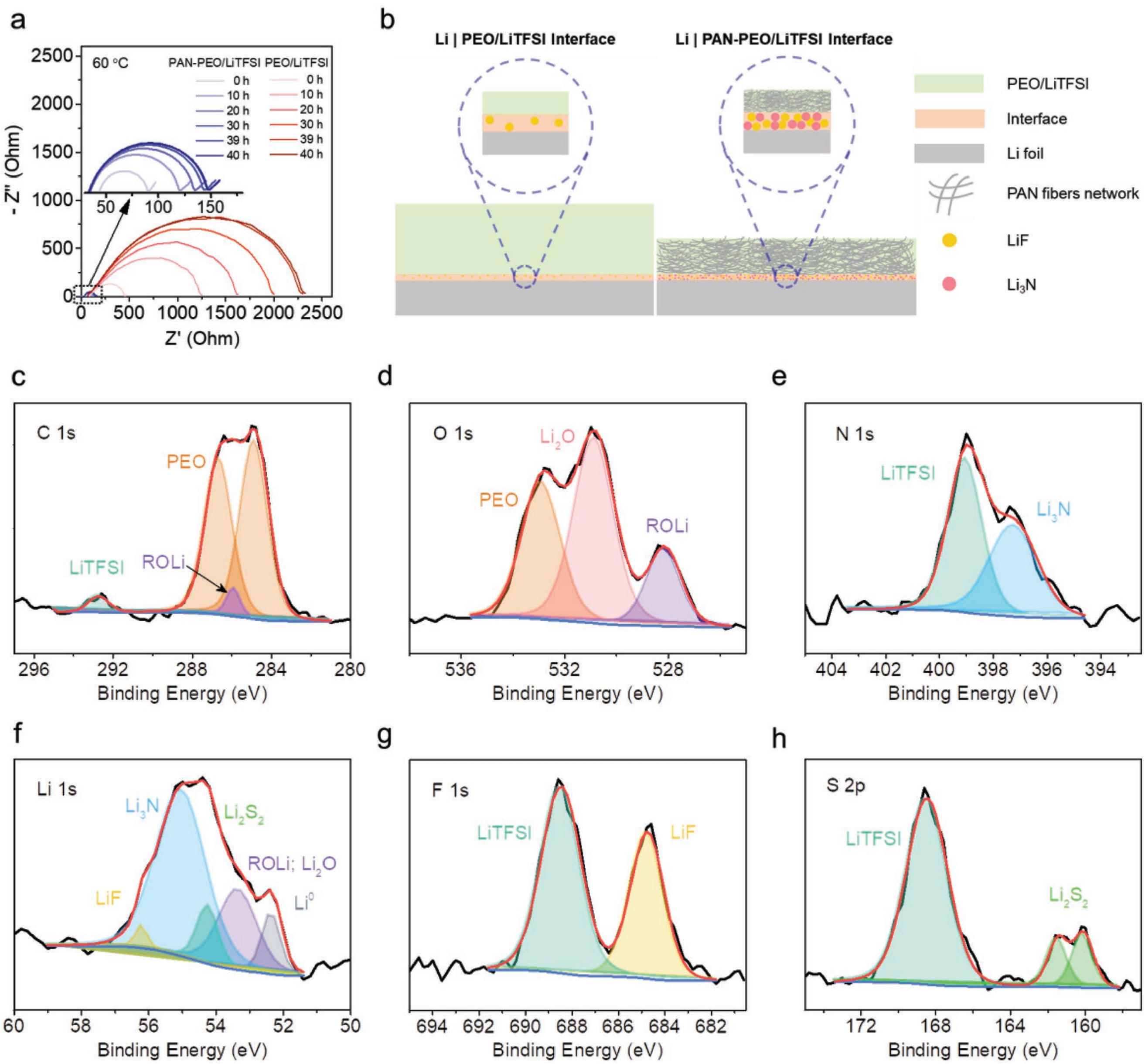

Figure 3. a) Electrochemical impedance spectroscopy plots of symmetrical Li—Li cells with PAN-PEO/LiTFSI SPE and PEO/LiTFSI electrolyte after rest at 60 °C for different times. Inset: zoom-in electrochemical impedance spectroscopy plots of symmetrical Li—Li cells with PAN-PEO/LiTFSI SPE. b) Schematic illustration for Li|PEO/LiTFSI interface[44,45] and Li|PAN-PEO/LiTFSI interface. c–h) XPS spectra of PAN-PEO/LiTFSI electrolyte|Li electrode interface: c) C 1s, d) O 1s, e) N 1s, f) Li 1s, g) F 1s, and h) S 2p.

with the electrolyte and provide a stable interface between PAN-based electrolyte and Li metal.[48–50,53–56] As for LiF, it can help suppress the penetration of Li dendrites into SSE, while its low electronic conductivity and intrinsic electrochemical stability block side reactions between the SSEs and Li.[53,57] Therefore, Li_3N and LiF can provide more stable interface between SPEs and Li metal. Besides, the calendaring process of the PAN host leads to a large interfacial contact area between PAN fibers and Li electrode, ensuring a large coverage of Li_3N formed at Li/SPE interfaces and, thus, a more stable interface than the bare PEO electrolyte. Therefore, with the formation of LiF and Li_3N at the interface between PAN-based electrolyte and Li metal, this interface is more stable during charge/discharge cycling, inhibiting the growth of lithium dendrites. As a result, long-term cycling at high current densities with low and stable overpotential was realized (Figure 2d), with an even higher critical current density (0.9 mA cm^{-2}) demonstrated at 60 °C (Figure 2b). As shown in Figure 3c–h, other components at the interface included: ROLi (C 1s peak at 285.8 eV, O 1s peak at 528.1 eV, and Li 1s peak at 53.3 eV), Li_2O (O 1s peak at 530.8 eV and Li 1s peak at 53.3 eV), and Li_2S_2 (Li 1s peak at 54.2 eV, S 2p peaks at 160.1 and 161.4 eV). Together with LiF and Li_3N, they constituted a complex interface layer, which helps in stabilizing the electrolyte/Li interface compared with non-LiF and Li_3N layers.

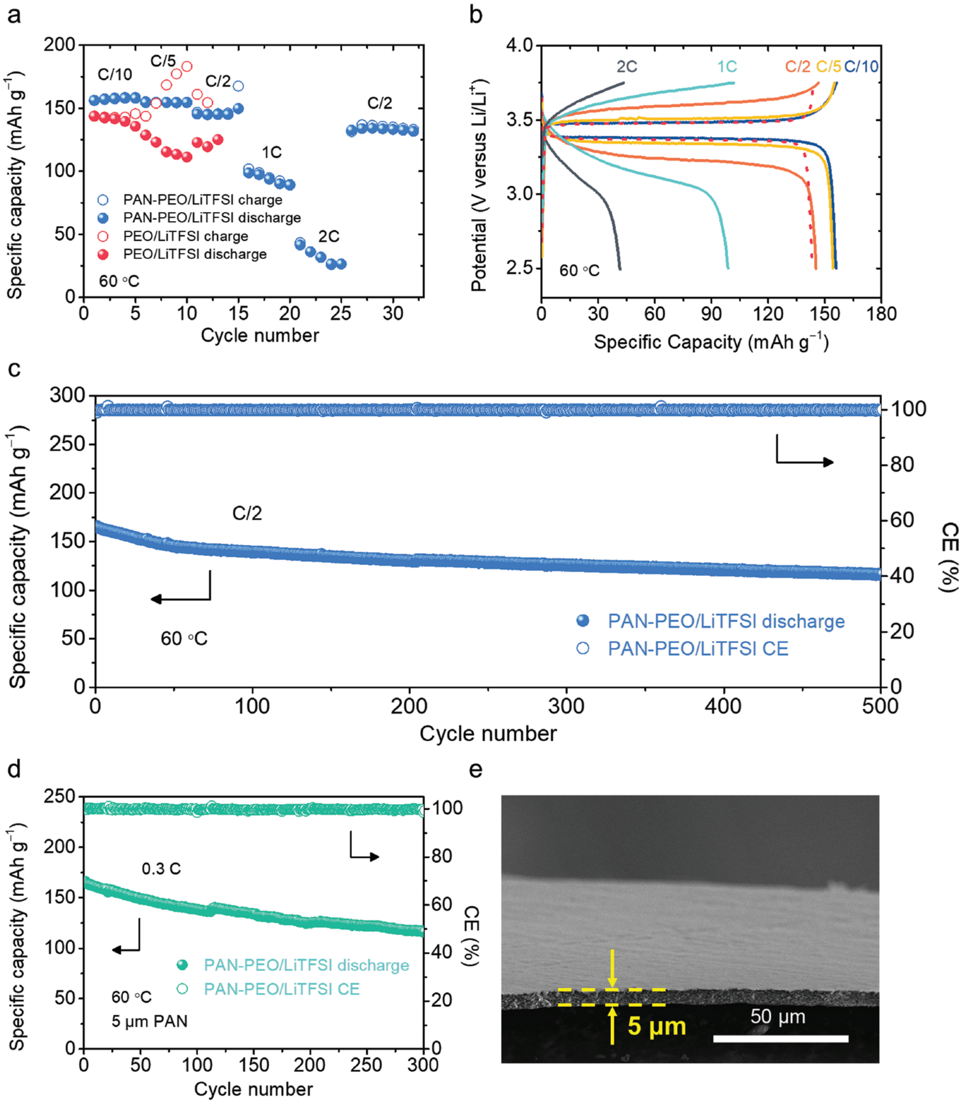

Figure 4. a) Rate performance of a Li/PEO/LiTFSI/LFP cell and a Li/PAN-PEO/LiTFSI/LFP cell, cycled at 60 °C. b) Voltage profiles of a Li/PAN-PEO/LiTFSI/LFP cell at different charging rates, cycled at 60 °C. Red dashed line is a Li/PEO/LiTFSI/LFP control cell at C/10 rate, at 60 °C. c) Cycling performance of Li/PAN-PEO/LiTFSI/LFP cell at C/2, cycled at 60 °C. d) Cycling performance of Li/PAN-PEO/LiTFSI/LFP cell with a 5 µm thick PAN-PEO/LiTFSI electrolyte at 0.3C, cycled at 60 °C. e) Cross-sectional SEM image of the ultrathin 5 µm PAN membrane.

To demonstrate the PAN-PEO/LiTFSI SPE's performance in a full battery configuration, we fabricated Li/PAN-PEO/LiTFSI/$LiFePO_4$ (LFP) batteries. The electrochemical performance of all-solid-state Li/LFP cells were also tested at 60 °C (**Figure 4**). Li/PAN-PEO/LiTFSI/LFP cells showed good rate performance, while Li/PEO/LiTFSI/LFP cells short circuited when the rate increased to C/5 (Figure 4a), exemplifying the plain PEO/LiTFSI electrolyte's comparative instability. This instability, as previously discussed, results from the inability of plain PEO/LiTFSI electrolyte to inhibit the growth of lithium dendrites, especially at high rates. However, with the help of the PAN membrane, lithium dendrites were effectively suppressed, allowing for a working rate of 2C. When cycling these cells at C/10, C/5, C/2, 1C, and 2C, the Li/PAN-PEO/LiTFSI/LFP all-solid-state LIB delivered high specific capacities of 155.9, 154.3, 145.3, 98.7, and 41.5 mAh g^{-1}, respectively. These cells also showed typical voltage profiles for LFP cathodes at different rates (Figure 4b). The Li/PAN-PEO/LiTFSI/LFP cell maintained low overpotentials of 92 mV at C/10 rates, reflecting the thin nature and low ionic resistance of PAN-PEO/LiTFSI membrane (Figure S5, Supporting Information). These results demonstrated that the rate capability of PAN-PEO/LiTFSI SPE was much better than that of PEO/LiTFSI SPE. Furthermore, benefitting from the special PAN host in the solid electrolyte, the all-solid-state Li/PAN-PEO/LiTFSI/LFP battery displayed high coulombic efficiency (CE) and stability at C/2, with the specific capacity remaining up to 70.0% after 500 cycles (Figure 4c). We also demonstrated Li/PAN-PEO/LiTFSI/LFP batteries with even thinner (5 µm) PAN-PEO/LiTFSI SPE (Figure S6, Supporting Information), which showed a stable cycling at 0.3C, with the specific capacity remaining up to 69.6% after 300 cycles (Figure 4d). This successful all-solid-state battery operation with a record-thinness electrospun polymer film (Figure 4e)

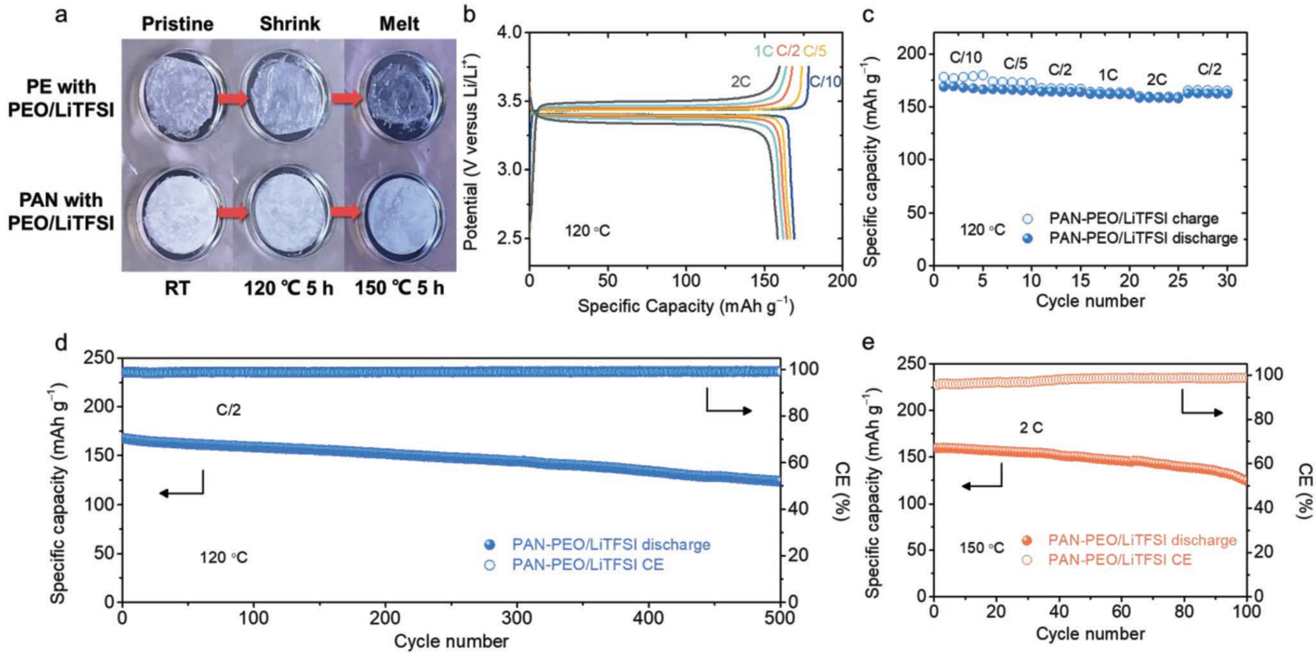

Figure 5. a) Photo images of PE-PEO/LiTFSI membrane and PAN-PEO/LiTFSI membrane before/after exposure to thermal shock at 120 °C for 5 h and 150 °C for 5 h. b) Voltage profiles of a Li/PAN-PEO/LiTFSI/LFP cell at different charging/discharging rates, cycled at 120 °C. c) Rate performance of a Li/PAN-PEO/LiTFSI/LFP cell, cycled at 120 °C. d) Cycling performance of Li/PAN-PEO/LiTFSI/LFP cell at C/2 rate, cycled at 120 °C. e) Cycling performance of Li/PAN-PEO/LiTFSI/LFP cell at 2C rate, cycled at 150 °C.

further indicates the promise of our design. In summary, the PAN-PEO/LiTFSI solid electrolyte showed great rate performance and cycling stability in an all-solid-state battery, even for an ultrathin thickness of 5 µm.

Good thermal stability is also a key requirement for high-safety LIBs. We accordingly compared the thermal stability of the PAN-PEO/LiTFSI to that of a PE separator infiltrated with PEO/LiTFSI (PE-PEO/LiTFSI). After exposure to high temperature conditions (120 °C, 5 h), the PE-PEO/LiTFSI shrank and melted after 5 h of exposure at 150 °C (**Figure 5**a). In contrast, no substantial changes in dimension or morphology were observed in the PAN-PEO/LiTFSI (Figure 5a). This was also to be confirmed by microscopic SEM images (Figure S7, Supporting Information); there was no obvious difference observed on the PAN-PEO/LiTFSI membrane before and after heat treatment at the testing temperature. A higher operating temperature of 200 °C was also reached (Figure S8, Supporting Information). These results indicate that the PAN-PEO/LiTFSI exhibits good thermal stability.

The excellent thermal stability of PAN-PEO/LiTFSI SPE ensures that PAN-PEO/LiTFSI based batteries can perform well at high temperature. To showcase this high temperature stability, we tested Li/PAN-PEO/LiTFSI/LFP all-solid-state batteries at 120 °C. As shown in Figure 5b, the Li/PAN-PEO/LiTFSI/LFP cells delivered excellent rate performance and maintained very low overpotentials of 32, 41, 59, 97, and 159 mV at C/10, C/5, C/2, 1C, and 2C rates, respectively. When cycled at C/10, C/5, C/2, 1C, and 2C, the Li/PAN-PEO/LiTFSI/LFP cells also delivered high specific capacities of 168.9, 166.5, 164.5, 162.1, and 158.5 mAh g^{-1}, respectively (Figure 5c). The specific capacity at C/10 was, in fact, very close to the theoretical capacity of LFP (170 mAh g^{-1}) and there was only a slight drop in specific capacity as the rate increased. These results indicate that these all-solid-state batteries working at high temperature not only achieved increased utilization of active material in the cathode due to improved polymer ionic conductivity (Figure S5, Supporting Information), but also displayed improved rate performance. Both of these improvements can be attributed to the excellent chemical and thermal stability of the PAN membrane; even at a high temperature of 120 °C, it still inhibited the growth of lithium dendrites and provided a stable electrolyte|Li metal interface, offering fast and stable lithium-ion transmission at high charge/discharge rates. Figure 5d shows the specific capacity and CE of the Li/PAN-PEO/LiTFSI/LFP cell at the rate of C/2 at 120 °C. The Li/PAN-PEO/LiTFSI/LFP cell shows very stable cycling for 500 cycles, with the specific capacity remaining up to 73.8% after 500 cycles. Thus, only ≈0.05% capacity decayed during each cycle, indicating excellent cycling stability. The all-solid-state cell with PAN-PEO/LiTFSI electrolyte also ran at an even higher temperature of 150 °C and a higher rate of 2C, and still showed good cycling efficiency and stability for 100 cycles (Figure 5e). Both temperature ranges are well outside the functional range of commonly used PE separators and conventional SPEs (e.g., PEO/LiTFSI), and these tests demonstrate the ease with which our PAN-based SPE overcomes the inherently poor thermal stability of SPEs for all-solid-state battery applications at even extreme conditions.

3. Conclusion

In summary, a PAN membrane-based SPE with high mechanical strength, good interfacial stability with Li metal, and excellent thermal stability can be easily achieved through electrospinning, followed by infiltration of PEO/LiTFSI. The modulus of PAN is five orders of magnitude higher than that of the plain PEO/LiTFSI electrolyte. The novel SPE demonstrates a stable SPE/Li interface, with interfacial resistance that is much lower and more stable than that of conventional PEO/LiTFSI|Li interfaces. As a result, the PAN-PEO/LiTFSI electrolyte showed excellent cycling stability at high current densities, effectively inhibiting lithium dendrites. This stability between our electrolyte and Li metal originates from the LiF and Li_3N formed at the electrolyte|Li metal interface. Furthermore, the PAN-PEO/LiTFSI solid electrolyte demonstrates a better rate performance and cycling stability than that of plain PEO/LiTFSI in Li/SSE/LFP cells. The electrospun PAN membrane also exhibits good thermal stability, which ensures that Li/PAN-PEO/LiTFSI/LFP all-solid-state batteries show excellent cycling stability at high temperatures up to 150 °C. This work accordingly provides an effective technique to prepare ultrathin, safe SPEs with high energy density, high temperature resistance, and a long lifespan. This work can also provide guiding principles in designing future high-performance SPEs working at high temperatures and inspire a more extensive research and application of SPEs.

4. Experimental Section

Chemicals and Materials: Polyacrylonitrile powder (PAN, Mw = 150000, Sigma Aldrich), dimethylformamide (DMF, Sigma Aldrich), PEO (Mw = 300000, Sigma Aldrich), LiTFSI (Solvay), acetonitrile (anhydrous, Sigma Aldrich), LFP powders (MTI), carbon black (Sigma Aldrich), Li foil (Sigma Aldrich).

Preparation of Electrospun PAN Membrane: The PAN powder was vacuum dried at 60 °C for 12 h before use. Then PAN electrospinning solution with the mass fraction of 12 wt% was obtained by dissolving the PAN polymer powder in the DMF solvent followed by mechanical and ultrasonic stirring at room temperature (RT) for 1.5 and 1.0 h, respectively. In our study, the PAN membrane was prepared by a single needle using the NE-1000 Programmable Single Syringe Pump. The electrospinning conditions were as follows: the PAN solution was electrospun at a voltage of 15 kV by a high voltage power supply (Gamma High Voltage Research, Inc.). The spinneret tip-to-collector distance was 15 cm and the feeding rate of the pump was set to 1 mL h^{-1}. The electrospinning temperature was maintained at ≈20 ± 5 °C and the humidity during the preparation was kept at ≈23 ± 5%. An aluminum foil was used as the collector for PAN nanofibers. A white uniform nanofibrous membrane with a certain thickness and strength was obtained on the surface of the aluminum foil. Then the electrospun PAN membrane was dried under vacuum at 60 °C to remove the residual solvent. Finally, the PAN membrane was treated by calendaring for use.

Preparation of SSE: PEO was mixed with LiTFSI and acetonitrile using a Thinky mixer (Thinky Cooperation). The EO to Li ratio was 10:1. Plain PEO/LiTFSI electrolytes were prepared by doctor blade casting followed by drying in a vacuum oven at 60 °C for 24 h and baking in an Ar-filled glove box at 70 °C for at least 48 h. PAN-PEO/LiTFSI solid electrolytes were obtained in a simple one-step process. The as-prepared PEO/LiTFSI/acetonitrile solution drops were dropped on both sides of the PAN membrane and then put in a 60 °C vacuum oven, kept vacuumed for 20 min to ensure the full infiltration of PEO/LiTFSI into the nanopores. The PAN-PEO/LiTFSI then underwent the same drying process as the regular PEO/LiTFSI membrane. PE-PEO/LiTFSI membrane was prepared by the same method as that of PAN-PEO/LiTFSI.

Preparation of Other Battery Components: LFP powders, PEO/LiTFSI, and carbon black (w:w:w = 60:25:15) were mixed in acetonitrile using a Thinky mixer. The LFP active material loading was ≈3.0 mg cm^{-2} and 0.5 mAh cm^{-2}. The slurry was then bladed on Al foil to render uniform coating, which was further dried in a vacuum oven at 60 °C for at least 48 h. Coin cells (2032 type, MTI) were made either with Li/SSE/Li or Li/SSE/LFP-type cells.

Materials Characterizations: SEM images were obtained with a Thermo Fisher Scientific Apreo S LoVac SEM. Mechanical tests were undertaken with a TA instrument Q800 DMA. XPS analysis was performed on a PHI VersaProbe 1. A symmetrical Li/PAN-PEO/LiTFSI/Li cell was cycled at 0.5 mA cm^{-2}, 0.25 mAh cm^{-2} for 100 cycles at 60 °C, and then disassembled. After removing PAN-PEO/LiTFSI electrolyte from Li electrode, the Li electrode surface was studied by XPS measurement. Another symmetrical Li/PEO/LiTFSI/Li cell was cycled at 0.3 mA cm^{-2}, 0.15 mAh cm^{-2} for 100 cycles at 60 °C, and then disassembled. After removing PEO/LiTFSI electrolyte from Li electrode, the Li electrode surface was also studied by XPS measurement. Thermal stability was measured in an Ar-filled glove box by heating PE-PEO/LiTFSI and PAN-PEO/LiTFSI at 120 °C for 5 h or 150 °C for 5 h (Figure 5a), or heating PE-PEO/LiTFSI and PAN-PEO/LiTFSI from 100 to 200 °C, after being increased by 10 °C, and kept for 5 min (Figure S8, Supporting Information).

Electrochemical Characterizations: Critical current density and long-term cycling of symmetrical Li—Li cells were conducted with a symmetrical Li/SSE/Li structure in coin cells (2032 type). Cells were cycled at low current density for the first few cycles for activation. Rate performance and long-term cycling of Li/LFP cells were conducted with a Li/SSE/LFP structure in coin cells (2032 type). Interfacial resistances between SSE with Li metal were tested with a symmetrical Li/SSE/Li structure in coin cells (2032 type). Ionic conductivity measurements were conducted with a symmetrical stainless steel (SS)/SSE/SS structure in coin cells (2032 type). All electrochemical measurements, such as electrochemical impedance spectroscopy and cycling tests, were carried out with Bio-logic VMP3 and LAND systems. All temperature-controlled experiments were tested inside an environmental chamber (BTU-133, ESPEC North America) using a high-precision thermometer (±0.1 °C). For the battery testing at 150 °C, a C-type clamp was used on both sides of coin cells to keep the constant pressure, and the cells were tested inside an environmental chamber (BTU-133, ESPEC North America) using a high-precision thermometer (±0.1 °C) in an Ar-filled glove box.

Acknowledgements

Y.M. and J.W. contributed equally to this work. This work was supported by Stanford University Funding. Y.M. acknowledges financial support from the China Scholarship Council.

Conflict of Interest

The authors declare no conflict of interest.

Data Availability Statement

The data that support the findings of this study are available from the corresponding author upon reasonable request.

Keywords

all-solid-state batteries, electrospun polyacrylonitrile matrix, high-temperature-resistant, solid polymer electrolytes, ultrathin

Received: November 28, 2021
Revised: January 23, 2022
Published online: February 25, 2022

[1] X.-B. Cheng, C.-Z. Zhao, Y.-X. Yao, H. Liu, Q. Zhang, *Chem* **2019**, *5*, 74.
[2] A. Manthiram, X. Yu, S. Wang, *Nat. Rev. Mater.* **2017**, *2*, 16103.
[3] P. Albertus, S. Babinec, S. Litzelman, A. Newman, *Nat. Energy* **2017**, *3*, 16.
[4] R. Chen, Q. Li, X. Yu, L. Chen, H. Li, *Chem. Rev.* **2020**, *120*, 6820.
[5] D. Lin, Y. Liu, Y. Cui, *Nat. Nanotechnol.* **2017**, *12*, 194.
[6] L. Fan, S. Wei, S. Li, Q. Li, Y. Lu, *Adv. Energy Mater.* **2018**, *8*, 1702657.
[7] S. Xia, X. Wu, Z. Zhang, Y. Cui, W. Liu, *Chem* **2019**, *5*, 753.
[8] Q. Zhao, S. Stalin, C.-Z. Zhao, L. Archer, *Nat. Rev. Mater.* **2020**, *5*, 229.
[9] C. Wang, K. Fu, S. Kammampata, D. McOwen, A. Samson, L. Zhang, G. Hitz, A. Nolan, E. Wachsman, Y. Mo, V. Thangadurai, L. Hu, *Chem. Rev.* **2020**, *120*, 4257.
[10] G. Xi, M. Xiao, S. Wang, D. Han, Y. Li, Y. Meng, *Adv. Funct. Mater.* **2020**, *31*, 2007598.
[11] Y. Kato, S. Hori, T. Saito, K. Suzuki, M. Hirayama, A. Mitsui, M. Yonemura, H. Iba, R. Kanno, *Nat. Energy* **2016**, *1*, 16030.
[12] X. Han, Y. Gong, K. Fu, X. He, G. Hitz, J. Dai, A. Pearse, B. Liu, H. Wang, G. Rubloff, Y. Mo, V. Thangadurai, E. Wachsman, L. Hu, *Nat. Mater.* **2017**, *16*, 572.
[13] Y.-G. Lee, S. Fujiki, C. Jung, N. Suzuki, N. Yashiro, R. Omoda, D.-S. Ko, T. Shiratsuchi, T. Sugimoto, S. Ryu, J. Ku, T. Watanabe, Y. Park, Y. Aihara, D. Im, I. Han, *Nat. Energy* **2020**, *5*, 299.
[14] F. Han, J. Yue, X. Zhu, C. Wang, *Adv. Energy Mater.* **2018**, *8*, 1703644.
[15] A. Christie, S. Lilley, E. Staunton, Y. Andreev, P. Bruce, *Nature* **2005**, *433*, 50.
[16] K. Harry, D. Hallinan, D. Parkinson, A. MacDowell, N. Balsara, *Nat. Mater.* **2014**, *13*, 69.
[17] X. Zhang, S. Wang, C. Xue, C. Xin, Y. Lin, Y. Shen, L. Li, C. Nan, *Adv. Mater.* **2019**, *31*, 1806082.
[18] D. Lin, W. Liu, Y. Liu, H. Lee, P.-C. Hsu, K. Liu, Y. Cui, *Nano Lett.* **2016**, *16*, 459.
[19] X. Zhang, J. Xie, F. Shi, D. Lin, Y. Liu, W. Liu, A. Pei, Y. Gong, H. Wang, K. Liu, Y. Xiang, Y. Cui, *Nano Lett.* **2018**, *18*, 3829.
[20] H. Xie, C. Yang, K. Fu, Y. Yao, F. Jiang, E. Hitz, B. Liu, S. Wang, L. Hu, *Adv. Energy Mater.* **2018**, *8*, 1703474.
[21] J. Wan, J. Xie, D. G. Mackanic, W. Burke, Z. Bao, Y. Cui, *Mater. Today Nano* **2018**, *4*, 1.
[22] K. J. Kim, M. Balaish, M. Wadaguchi, L. Kong, J. L. M. Rupp, *Adv. Energy Mater.* **2020**, *11*, 2002689.
[23] X. Miao, H. Wang, R. Sun, C. Wang, Z. Zhang, Z. Li, L. Yin, *Energy Environ. Sci.* **2020**, *13*, 3780.
[24] Q. Zhang, K. Liu, F. Ding, X. Liu, *Nano Res.* **2017**, *10*, 4139.
[25] D. Hallinan, N. Balsara, *Annu. Rev. Mater. Res.* **2013**, *43*, 503.
[26] D. Lin, P. Yuen, Y. Liu, W. Liu, N. Liu, R. Dauskardt, Y. Cui, *Adv. Mater.* **2018**, *30*, 1802661.
[27] X. Zhang, T. Liu, S. Zhang, X. Huang, B. Xu, Y. Lin, B. Xu, L. Li, C.-W. Nan, Y. Shen, *J. Am. Chem. Soc.* **2017**, *139*, 13779.
[28] M.-T. Rodrigues, G. Babu, H. Gullapalli, K. Kalaga, F. Sayed, K. Kato, J. Joyner, P. Ajayan, *Nat. Energy* **2017**, *2*, 17108.
[29] S. Randau, D. Weber, O. Kötz, R. Koerver, P. Braun, A. Weber, E. Ivers-Tiffée, T. Adermann, J. Kulisch, W. Zeier, F. Richter, J. Janek, *Nat. Energy* **2020**, *5*, 259.
[30] Z. Jiang, S. Wang, X. Chen, W. Yang, X. Yao, X. Hu, Q. Han, H. Wang, *Adv. Mater.* **2020**, *32*, 1906221.
[31] W. Zhou, S. Wang, Y. Li, S. Xin, A. Manthiram, J. Goodenough, *J. Am. Chem. Soc.* **2016**, *138*, 9385.
[32] T. Liu, Y. Zhang, X. Zhang, L. Wang, S.-X. Zhao, Y.-H. Lin, Y. Shen, J. Luo, L. Li, C.-W. Nan, *J. Mater. Chem. A* **2018**, *6*, 4649.
[33] F. Zhao, J. Liang, C. Yu, Q. Sun, X. Li, K. Adair, C. Wang, Y. Zhao, S. Zhang, W. Li, S. Deng, R. Li, Y. Huang, H. Huang, L. Zhang, S. Zhao, S. Lu, X. Sun, *Adv. Energy Mater.* **2020**, *10*, 1903422.
[34] J. Wan, J. Xie, X. Kong, Z. Liu, K. Liu, F. Shi, A. Pei, H. Chen, W. Chen, J. Chen, X. Zhang, L. Zong, J. Wang, L.-Q. Chen, J. Qin, Y. Cui, *Nat. Nanotechnol.* **2019**, *14*, 705.
[35] R. Bouchet, S. Maria, R. Meziane, A. Aboulaich, L. Lienafa, J.-P. Bonnet, T. Phan, D. Bertin, D. Gigmes, D. Devaux, R. Denoyel, M. Armand, *Nat. Mater.* **2013**, *12*, 452.
[36] R. Khurana, J. Schaefer, L. Archer, G. Coates, *J. Am. Chem. Soc.* **2014**, *136*, 7395.
[37] J. Wu, Z. Rao, Z. Cheng, L. Yuan, Z. Li, Y. Huang, *Adv. Energy Mater.* **2019**, *9*, 1902767.
[38] Y. Cui, J. Wan, Y. Ye, K. Liu, L.-Y. Chou, Y. Cui, *Nano Lett.* **2020**, *20*, 1686.
[39] X. Li, W. Chen, Q. Qian, H. Huang, Y. Chen, Z. Wang, Q. Chen, J. Yang, J. Li, Y.-W. Mai, *Adv. Energy Mater.* **2021**, *11*, 2000845.
[40] Z. Zhang, Y. Huang, G. Zhang, L. Chao, *Energy Storage Mater.* **2021**, *41*, 631.
[41] J. Ping, H. Pan, P.-P. Hou, M.-Y. Zhang, X. Wang, C. Wang, J. Chen, D. Wu, Z. Shen, X.-H. Fan, *ACS Appl. Mater. Interfaces* **2017**, *9*, 6130.
[42] X. Cao, J. Cheng, X. Zhang, D. Zhou, Y. Tong, *Int. J. Electrochem. Sci.* **2020**, *15*, 677.
[43] X.-L. Wu, Y.-H. Li, N. Wu, S. Xin, J.-H. Kim, Y. Yan, J.-S. Lee, Y.-G. Guo, *Solid State Ionics* **2013**, *245-246*, 1.
[44] C. Xu, B. Sun, T. Gustafsson, K. Edström, D. Brandell, M. Hahlin, *J. Mater. Chem. A* **2014**, *2*, 7256.
[45] I. Ismail, A. Noda, A. Nishimoto, M. Watanabe, *Electrochim. Acta* **2001**, *46*, 1595.
[46] P. Jaumaux, Q. Liu, D. Zhou, X. Xu, T. Wang, Y. Wang, F. Kang, B. Li, G. Wang, *Angew. Chem., Int. Ed.* **2020**, *59*, 9134.
[47] H. Xu, Y. Li, A. Zhou, N. Wu, S. Xin, Z. Li, J. Goodenough, *Nano Lett.* **2018**, *18*, 7414.
[48] K. Park, J. Goodenough, *Adv. Energy Mater.* **2017**, *7*, 1700732.
[49] Y. Li, Y. Sun, A. Pei, K. Chen, A. Vailionis, Y. Li, G. Zheng, J. Sun, Y. Cui, *ACS Cent. Sci.* **2018**, *4*, 97.
[50] M. Yan, J.-Y. Liang, T.-T. Zuo, Y.-X. Yin, S. Xin, S.-J. Tan, Y.-G. Guo, L.-J. Wan, *Adv. Funct. Mater.* **2019**, *30*, 1908047.
[51] K. Shi, Z. Wan, L. Yang, Y. Zhang, Y. Huang, S. Su, H. Xia, K. Jiang, L. Shen, Y. Hu, S. Zhang, J. Yu, F. Ren, Y.-B. He, F. Kang, *Angew. Chem., Int. Ed.* **2020**, *59*, 11784.
[52] W. Li, G. Wu, C. Araújo, R. Scheicher, A. Blomqvist, R. Ahuja, Z. Xiong, Y. Feng, P. Chen, *Energy Environ. Sci.* **2010**, *3*, 1524.
[53] X. Ji, S. Hou, P. Wang, X. He, N. Piao, J. Chen, X. Fan, C. Wang, *Adv. Mater.* **2020**, *32*, 2002741.
[54] Q. Dong, B. Hong, H. Fan, H. Jiang, K. Zhang, Y. Lai, *ACS Appl. Mater. Interfaces* **2020**, *12*, 627.
[55] K. Park, B.-C. Yu, J. Goodenough, *Adv. Energy Mater.* **2016**, *6*, 1502534.
[56] C. Wang, X. Sun, L. Yang, D. Song, Y. Wu, T. Ohsaka, F. Matsumoto, J. Wu, *Adv. Mater. Interfaces* **2021**, *8*, 2001698.
[57] X. Fan, X. Ji, F. Han, J. Yue, J. Chen, L. Chen, T. Deng, J. Jiang, C. Wang, *Sci. Adv.* **2018**, *4*, eaau9245.